Materials Horizons

ROYAL SOCIETY OF CHEMISTRY

COMMUNICATION

View Article Online
View Journal | View Issue

Cite this: *Mater. Horiz.*, 2025, 12, 3841

Received 7th November 2024,
Accepted 5th March 2025

DOI: 10.1039/d4mh01598c

rsc.li/materials-horizons

Hyaluronic acid-based hydrogels modulate neuroinflammation and extracellular matrix remodelling in multiple sclerosis: insights from a primary cortical cell model†

Sergio Martin-Saldaña, *[a] Mansoor Al-Waeel,[a] Enrico Bagnoli, [ab] Merari Tumin Chevalier,[a] Yazhong Bu,[a] Christopher Lally,[a] Una Fitzgerald[ab] and Abhay Pandit*[ab]

Multiple sclerosis (MS) is the main neurodegenerative disorder among young adults. Cortical involvement in MS has emerged as an important determinant of disease progression. Although inflammation is recognized as a key feature, the mechanisms of cortical pathology are still poorly understood. The critical role of the extracellular matrix (ECM) in the development and homeostasis of the central nervous system (CNS) and hyaluronic acid (HA) *in primis* has been emphasized. HA synthesis increases during neuroinflammation in the cortex, mostly through hyaluronan synthase 2 (HAS2), generating an ECM scar on demyelinated axons. Here, we aimed to prove the potential role of an external source of HA in CNS inflammation, specifically in a complex *in vitro* model of neuroinflammation using primary cortical cells (PCC). We engineered and characterized a battery of cross-linked HA-based hydrogels and tested their impact on LPS-triggered inflammation in PCC. The performance of the tested HA scaffolds is promising for their potential use *in vivo*, exhibiting an appealing anti-inflammatory response. We also studied the effect of the crosslinked HA hydrogels on hyaluronan metabolism and catabolism markers, showing a significant decrease in HAS2 expression, which could have a critical impact on scar generation in demyelinated axons. Finally, we analyzed the effect of the degradation products of the HA constructs, shedding light on the unsolved debate about the potential dual effect of HA-based materials on the CNS depending on their molecular weight. Altogether, our results contribute to baseline knowledge regarding the use of HA-based materials in the context of CNS inflammatory disorders.

New concepts

We tested the effect of a high molecular weight (HMW) hyaluronic acid (HA) hydrogel, on HA metabolism and catabolism after neuroinflammation in a Primary Cortical Cell (PCC) *in vitro* model. While HA systems have been tested in the context of central nervous system (CNS) pathologies, their effect on extracellular matrix (ECM) remodelling, specially related to hyaluronan metabolism, are rarely explored. ECM remodelling is critical in neuroinflammatory driven disorders in the CNS due to the formation of HA scars that avoid a proper recovery of the damaged tissue. The engineered hydrogels downregulated neuroinflammation in a consistent manner up to 7 days post treatment. Interestingly, HA hydrogels downregulated hyaluronan synthase 2 (HAS2), the key enzyme in charge of HA synthesis after an inflammatory insult in the cortex, suggesting a potential effect on avoiding the generation of HA scars. This will allow oligodendrocytes to reach the demyelinated axons to remyelinate them. Moreover, we tested the effect of the HA hydrogel's degradation products and LMW HA over PCC showing no detrimental or pro-inflammatory effect in the case of LMW HA. This shed some light on the unsolved debate regarding the potential dual effect of HA-based materials on the CNS, depending on its molecular weight.

1. Introduction

Inflammation is a common feature of most neurodegenerative disorders and plays a pivotal role in Alzheimer's disease, Parkinson's disease, stroke, multiple sclerosis (MS), and brain cancers.[1,2] Among them, MS, a chronic inflammatory immune-mediated demyelinating disease of the CNS, has a bigger impact on patient quality of life and is frequently diagnosed between 20 and 40 years of age. At present, MS affects more than 1.2 million people in Europe and 2.8 million worldwide and is the main non-traumatic cause of disability in young adults. MS is a complex and highly variable disease that can be defined based on symptoms. The most common is relapsing-remitting MS (RRMS), which causes flare-ups (relapses or attacks) of new or old symptoms, followed by periods of remission. In many cases, RRMS eventually progresses to secondary progressive MS (SPMS), where nerve damage accumulates and symptoms worsen. Moreover, MS symptoms could start off slowly and gradually worsen over time

[a] *CÚRAM Research Ireland Center for Medical Devices, University of Galway, Galway H91 W2TY, Ireland. E-mail: s.martinsaldana@ictp.csic.es, smartinsaldana@gmail.com, abhay.pandit@universityofgalway.ie*
[b] *Galway Neuroscience Centre, University of Galway, Galway H91 W2TY, Ireland*

† Electronic supplementary information (ESI) available. See DOI: https://doi.org/10.1039/d4mh01598c

from the beginning of the disease, in so-called primary progressive MS (PPMS), without any periods of clear relapses or remission. Most of the available treatments for MS have modest effects on relapse symptoms but are not effective in modifying disease progression.[3] With no available cure nowadays, most injectable or oral drugs can only slow disease progression. Moreover, since the blood brain barrier (BBB) remains intact in MS, the systemic administration route is highly inefficient.[2] In this context, there is a critical need to develop new formulations that can improve drug delivery to the brain in an MS pathological context and reduce systemic side effects.

In the last two decades, the critical role of the ECM in the development and homeostasis of the CNS has emerged.[4–6] The main components of neural ECM include chondroitin sulfate proteoglycans (CS), tenascin-R, and hyaluronic acid (HA), which are synthesized by both neurons and glial cells.[6] These are tightly regulated under physiological conditions and shape both neuronal and glial functions. Their synthesis increases during pathological processes such as neuroinflammation and neurodegeneration, resulting in the formation of growth-non permissive environment.[4,7] Indeed, targeting expression of specific ECM molecules has been widely exploited in other diseases such as fibrosis or cancer, with promising therapeutic outcomes, but has been underexplored in the context of the CNS disorders.[8] High molecular weight (HMW) HA is especially abundant during CNS development and remains ubiquitous in adult ECM.[9] Changes in HA content, the balance between HMW and low molecular weight (LMW), and its metabolism have been related to several CNS pathological conditions, and these changes disrupt repair by endogenous neural stem cells. HA has been successfully used in recent years with many different applications in biomedicine, including CNS disorders, but their effect on intrinsic ECM remodelling is far from being fully understood.[10] Endogenously synthesized HA accumulates at sites of autoimmune inflammation, including white matter lesions in MS, generating a scar in the demyelinated axons preventing remyelination mechanisms.[4] The treatment with 4-methylumbelliferone (4-MU), a potent inhibitor of HA synthesis, has shown decreases the incidence of experimental autoimmune encephalomyelitis (EAE) and reduces the severity of the disease, suggesting that HA synthesis is crucial for disease progression.[7]

In this study, we aimed to test the role of HA interactions in the onset of neuroinflammation using different HA constructs. We hypothesized that crosslinked HA-based hydrogels would have a critical impact on the resolution of neuroinflammation. Hence, we aimed to test an external source of cross-linked HA constructs that could modulate endogenous HA synthesis led by astrocytes by downregulating astrogliosis and reducing the severity of the inflammatory response. This downregulation in intrinsic HA synthesis from astrocytes, mostly mediated by hyaluronan synthase 2 (HAS2) in the cortex, will avoid its deposition and scar generation in demyelinated axons. This allows oligodendrocytes to remyelinate injured axons after an inflammatory insult. Furthermore, we will shed some light on the unsolved debate regarding the potential dual effect of HA-based materials on the CNS, depending on its molecular weight. Altogether, our results contribute to the baseline knowledge for the use of HA-based materials in the context of CNS inflammatory disorders.

2. Experimental section

2.1. Hydrogel preparation and characterization

2.1.1. Hydrogel preparation. HMW sodium hyaluronate (1 MDa, Lifecore Biomedical, Minnesota, USA) was dissolved at different concentrations (0.5, 1, 2, 5, 7.5, 10, and 20 mg mL^{-1}) in 1 mL (2-(*N*-morpholino)ethanesulfonic acid) (MES; Merck, Darmstadt, Germany) buffer (pH 5.5) with stirring. After complete mixing, 4-(4,6-dimethoxy-1,3,5-triazin-2-yl)-4-methylmorpholinium chloride (DMTMM) was added at a 20% w/w ratio with respect to HA to activate the carboxylic groups of the polymer. Thus, it was mixed with various final concentrations of 4-arm polyethylene glycol-amine (4-arm PEG-NH_2; Merck, Darmstadt, Germany) (2000 Da), mainly in 1 : 1 and 2 : 1 w/w ratios with respect to HA, to initiate cross-linking through DMTMM-activated amidation. Finally, the mixed components were kept overnight at 37 °C to allow crosslinking. The formulations of 0.5, 1, and 2 mg mL^{-1} were too diluted, and crosslinking did not occur in a homogenous manner. In contrast, the 20 mg mL^{-1} formulation was highly viscous, and its manipulation and further crosslinking were not possible. Thus, these four formulations were excluded from further testing because of their inability to form crosslinked hydrogels. To ensure reproducibility and uniformity among replicates, hydrogels were sectioned with a 10 mm biopsy-punch to obtain the final hydrogels. After complete fabrication, the HA hydrogels were washed in Phosphate buffer saline (PBS, Merck, Darmstadt, Germany) to remove non-reactant components, freeze-dried, and stored at 4 °C for further analyses.

2.1.2. Micro and macrostructure by scanning electron microscopy. The morphology of the crosslinked HA hydrogels was analyzed using field-emission scanning electron microscopy (FESEM, Hitachi SU 8000 TED). Briefly, samples of the same volume were frozen with liquid N_2, followed by cryosectioning to analyze the cross-section of the HA hydrogels. Subsequently, samples were prepared over a carbon tape disk with subsequent coating with a gold–palladium alloy (80 : 20).

2.1.3. Fourier transform infrared spectroscopy. FTIR was used to study the characteristic bands of all constituents of the proposed HA hydrogels. Infrared spectroscopy was performed in attenuated total reflection (ATR) mode using an IR 640 spectrophotometer (Varian). Samples were analyzed at room temperature using 16 scans with a resolution of 4 cm^{-1}.

2.1.4. Mechanical properties by rheology. Rheological analysis was performed using a modular compact rheometer (MCR-102, Anthon Paar) equipped with a Ø 25 mm stainless-steel parallel plate geometry and an electrically heated plate.[11] The operation temperature was maintained at 37 °C in the following measurements. The mechanical properties of the hydrogels were measured by recording their storage (G') and loss (G'') moduli as a function of time. The frequency sweep was recorded

at a frequency of 1 Hz, with a strain set at 1%. All experiments were performed at least in triplicate.

2.1.5. Swelling behaviour in ACSF. The swelling behavior of crosslinked HA hydrogels was determined by incubation in artificial cerebrospinal fluid (ACSF). Briefly, HA hydrogels were initially weighed (W_0) and incubated in ACSF at 37 °C in an incubator with orbital shaking (300 rpm). The medium was replenished with freshly prepared ACSF every three days. The hydrogels were recovered after 15′, 30′, 45′, 1 h, 2 h, 4 h, 6 h, 8 h, 12 h, 1 d, 3 d, 4 d, 6 d, 7 d, 8 d, 9 d, 14 d, 21 d and 28 d by removing all supernatants and were weighed. The weight of the HA gels (W_t) at each time point was measured, and the weight-fold change of the remaining hydrogels (wt) was calculated using the following eqn (1):

$$\text{wt} = W_t \times 1 \div W_0 \quad (1)$$

Maximum swelling was determined after 24 hours of incubation in ACSF, as most of the formulations reached maximum swelling at that time.

2.1.6. Enzymatic degradation on ACSF over time. The stability of the optimally crosslinked HA hydrogel was determined by enzymatic degradation. Briefly, HA hydrogels were weighed (W_0) and incubated in ACSF containing bovine hyaluronidase (HYAL; Merck, Darmstadt, Germany; 100 U mL^{-1}) at 37 °C with orbital shaking. The degradation medium was replenished with ACSF containing freshly prepared HYAL enzyme solution every three days. The hydrogels were recovered after 1 h, 2 h, 4 h, 6 h, 8 h, 12 h, 1 d, 3 d, 4 d, 6 d, 7 d, 8 d, 9 d, 14 d, 21 d and 28 d by removing the supernatant and were weighed. The weight of the HA gels (W_t) at each time point was measured and the weight percentage of the remaining hydrogels (wt%) was calculated using the following eqn (2):

$$\text{wt\%} = W_t \times 100 \div W_0 \quad (2)$$

2.2. Cell culture

2.2.1. Rat cortical postnatal mixed culture. Research and animal procedures were performed in accordance with the European (EU) guidelines (2010/63/UE) by a competent and trained operator, and were approved by the Animal Care Research Ethics Committee (ACREC) of the University of Galway. Every effort was made to minimize animal suffering and to reduce the number of animals used.

Sprague-Dawley rat pups (P10) were sacrificed with modifications of the protocol published by Mathew *et al.*[12] Cortex was harvested from the brain and chopped at 300 μm space using a Mc Tissue Chopper. The extracted tissue was then incubated in a papain-based dissociation solution (Worthington Biochemical Corp., New Jersey, USA), for one hour at 37 °C to proceed with trituration, strain, centrifugation, and cell counting. Cells were seeded in 12 or 24-well plates (3×10^5 cells per well, or 1.5×10^5 cells per well respectively) pre-coated with poly-L-lysine (PLL) and supplemented with Dulbecco's modified Eagle's medium/F12 (DMEM/F12, D6421, Sigma-Aldrich, Dublin, Ireland) supplemented with 6 g L^{-1} of D-glucose, 100 μg mL^{-1} of Primocin™ (InvivoGen®, Toulouse, France), 2 mM of L-glutamine (Sigma®, Wicklow, Ireland), 10 mL L^{-1} of fetal bovine serum (FBS), and 20 mL L^{-1} of B27® supplement (17504-044, Gibco™, NY, US). Media was replaced every other day for the duration of the culture.

2.2.2. LPS-induced cortical inflammatory model. After 7 days *in vitro*, the medium was refreshed with complete medium, and the cells were treated with lipopolysaccharide (LPS) (100 ng mL^{-1}). On the day after LPS treatment, different HA formulations were added to the culture. HA hydrogels were prepared under sterile conditions the day before the experiment, as described in Section 2.1.1. The prepared formulations were washed at least three times in sterile PBS before use.

Cells were exposed to conditioned media for 1, 3, or 7 days to determine their effects. After the stimulation periods, the culture medium was recovered and stored at −20 °C for further analysis.

2.2.3. Metabolic activity. Cell metabolic activity was evaluated using the alamarBlue™ protocol (Thermo Fisher). Briefly, 300 μL of 10% alamarBlue™ was added per well, incubated for 3 h at 37 °C (5% CO_2, humidity), and the solution was collected, transferred to 96 well plates, and measured using a plate reader (Thermo Fisher, λ_{ex} 545 nm, λ_{em} 590 nm).

2.2.4. DNA quantification. The cell dsDNA content was evaluated using the PicoGreen™ assay after metabolic activity assessment. Briefly, a known volume of ultrapure water was added to each well, and after three freeze–thaw cycles, the samples were used following the manufacturer's protocol (PicoGreen™ Assay, Protocol ND-3300, Thermo Scientific). The ratio of metabolic activity to dsDNA content was calculated. Both determinations were performed at least three times in the same experiment and were performed in at least three independent experiments ($N > 3$).

2.2.5. Nitrite assay. The Griess reagent kit for nitrite quantification (Invitrogen) was used to quantify the nitrite species released by the cells following incubation with the different treatments. Briefly, 150 μL of the sample or nitrite standard was added to each well of a clear 96-well plate and incubated for 30 min at room temperature in the dark with Griess reagents. The absorbance was read at 548 nm, and the nitrite concentration in μM was extrapolated from the standard curve and displayed in the graph without normalization.

2.2.6. Cytokine release analysed by multiplex ELISA. The response of PCCs and LPS-exposed PCCs after HA treatment was studied using Multiplex ELISA according to the manufacturer's specifications (Meso Scale Diagnostics LLD, MSD). Briefly, pro-inflammatory (TNF-α, IL-1β, IFN-γ, IL-6, and KC/GRO) and anti-inflammatory (IL-10, IL-13, and IL-4) cytokines were quantified in the recovered culture media after one day. Two technical replicates were assessed for four independent experiments.

2.3. Immunocytochemistry

PCC cultures intended for imaging analysis were seeded onto PLL-coated coverslips in 12-well plates and received the same treatments described before and fixed at the desired time points (1, 3, and 7D post-treatment). Briefly, the medium was

removed, cells were washed with PBS, exposed for the desired time to 10% formalin, and washed again after fixation. The fixed cells were permeabilized by incubation in 0.2% Triton X-100 in PBS, followed by washing with PBS. Non-specific binding was blocked with 1% bovine serum albumin (BSA; Merck, Darmstadt, Germany) in PBS solution for one hour at room temperature (RT). Primary antibody mouse anti-GFAP (1 : 500, Sigma Aldrich), rabbit anti-Iba-1 (1 : 200, Dako), rabbit anti-β-tubulin III (1 : 500, ABCAM), mouse anti-olig-2 (1 : 200, Sigma Aldrich), mouse anti-myelin basic protein (MBP) (1 : 200, Sigma Aldrich), rabbit anti-CD44 (1 : 100 ABCAM), rabbit anti-HAS1 (1 : 50 ABCAM), and mouse anti HAS-2 (1 : 100 ABCAM) were prepared in blocking buffer and added to the plates, which were incubated overnight at 4 °C under stirring. After washing, cells were incubated with secondary antibodies Alexa Fluor® 488 (1 : 500, Thermo Scientific™, A-10667) and Alexa Fluor® 546 (1 : 500, Thermo Scientific™, A11035) for one hr at RT. After washing, the cells were incubated in DAPI (1 : 2000, Thermo Scientific™) for five minutes at RT and coverslips were mounted onto glass slides using a fluoromount and observed under a confocal microscope (Olympus FluoView 3000 system). Images were processed using ImageJ software (W. RasBand, National Institute of Health, Bethesda, USA).

2.4. Proteome profiler

The relative expression of chemokines, pro- and anti-inflammatory cytokines, and growth factors secreted by PCCs and LPS-exposed PCCs after HA treatment was determined using the Rat XL Cytokine Proteome Profiler™ Array kit, according to the manufacturer's instructions (ARY030, R&D SYSTEMS). The signals relative to protein expression were recorded on X-ray films (CL-XPosure™ Film, Thermo Scientific™, 34090), which were further analyzed using the Image Studio™ Lite software as pixel density. Further, each analyte calculated the 'mean pixel density,' and the data were plotted as a heatmap. Hierarchical clustering of the data was performed using Morpheus software (**https://software.broadinstitute.org/morpheus**).

2.5. RT-PCR

Gene expression in treated and control PCC was assessed by qRT-PCR. Briefly, total RNA was isolated from the organotypic slices using a phase separation method. The quality, purity, and concentration of the extracted RNA were measured using a NanoDrop 2000c spectrophotometer (Thermo Fisher). cDNA was synthesized using the Qiagen® RT^2 first-strand kit, according to the manufacturer's instructions, and 500 ng of RNA was used as a template for each reaction. The obtained cDNA was diluted 1 in 5 in molecular biology-grade H_2O before use in qRT-PCR. Briefly in each well of a 384 well plate, 2 μL of diluted cDNA, 7.5 μL of Taqman master mix, 0.75 μL of primer mix (Table 1, forward and reverse) and 4.75 μL of water were combined. Each sample was analyzed in triplicate. The results were quantified using a comparative Ct method and normalized using three housekeeping genes (B2M, Rplp0, and HPRT).

Table 1 Primer sequences used for qRT-PCR

HYAL1-F	5′-CCA GGA TTT CTG GTG GAA GA-3′
HYAL1-R	5′-CCA CAG GAC TTG CTC TAG-3′
HYAL2-F	5′-CCT CTG GGG CTT CTA CCT CT-3′
HYAL2-R	5′-CTG AAC ACG GAA GCT CAC AA-3′
HYAL3-F	5′-TCA GCT GCC ACT GTT ACT GG-3′
HYAL3-R	5′-TGA CTC TCC CTG GAA CTG CT-3′
HAS1-F	5′-GCG GGC TTG TCA GAG CTA-3′
HAS1-R	5′-AGA GCG ACA GAA GCA CCA-3′
HAS2-F	5′-GTG ATG ACA GGC ATC TCA-3′
HAS2-R	5′-GCG GGA AGT AAA CTC GA-3′
HAS3-F	5′-CAG CCT GCA CCA TCG A-3′
HAS3-R	5′-AGA GGT GGT GCT TAT GGA-3′
CD44-F	5′-GTG GGC CAA CAA AGA ACA CT-3′
CD44-R	5′-TGG AGC AGG CCC AAA TAT AG-3′
RHAMM-F	5′-GAA AGG GAA GAAGGC TGA AC-3′
RHAMM-R	5′-TGC CAA AAT CTG ATG CTG AA-3′
TSG-6-F	5′-TCA CAT TTC AGC CAC TGC TC-3′
TSG-6-R	5′-AGA CCG TGC TTC TCT GTG GT-3′

2.6. Effect of HA degradation products on PCCs

HA hydrogels were incubated as described in Section 2.1.6. Afterwards, 1.5 × 10^5 cells per well were seeded into 24-well plates pre-coated with PLL. After differentiation, the medium was refreshed, and the cells were treated with LPS (100 ng mL^{-1}), HA hydrogel degradation products, or HYAL (100 U mL^{-1}) previously incubated under the same conditions. Cells were exposed to conditioned media for 24 h to determine any effect. After the stimulation period, the culture medium was recovered and stored at −20 °C for further analysis.

2.7. Statistical analysis

Graphs and figures were created using the GraphPad® software. Statistical differences in histochemical quantification were analyzed using GraphPad Software. One-way ANOVA was performed where appropriate, followed by Tukey's or Dunnett's *post hoc* tests. The mean and standard deviation (SD) were calculated for all groups. All error bars indicate SD.

3. Results and discussion

3.1. HA-Based crosslinked hydrogels exhibited appealing properties for their use on the CNS

ECM remodeling during neuroinflammation is a well-known process. However its role on disease onset is still poorly understood.[7] HA is a primary component of the brain ECM, playing a pivotal role in regulating cell behavior through migration, proliferation, differentiation, and inflammation, thus contributing to maintain CNS homeostasis.[13] ECM equilibrium is disrupted during an inflammatory insult, which leads to a remodeling that inhibits homeostatic processes that support critical tissue health and functionality. Hence, HA-based constructs have been widely investigated to ameliorate inflammation-driven damage.[14,15] HA's effectiveness in tissue healing and regeneration is primarily attributed to its impact on cell signaling and the ease of customizing chemical and mechanical properties.

Herein, HA-based crosslinked hydrogels were fabricated to improve the retention and physicochemical properties of HA.

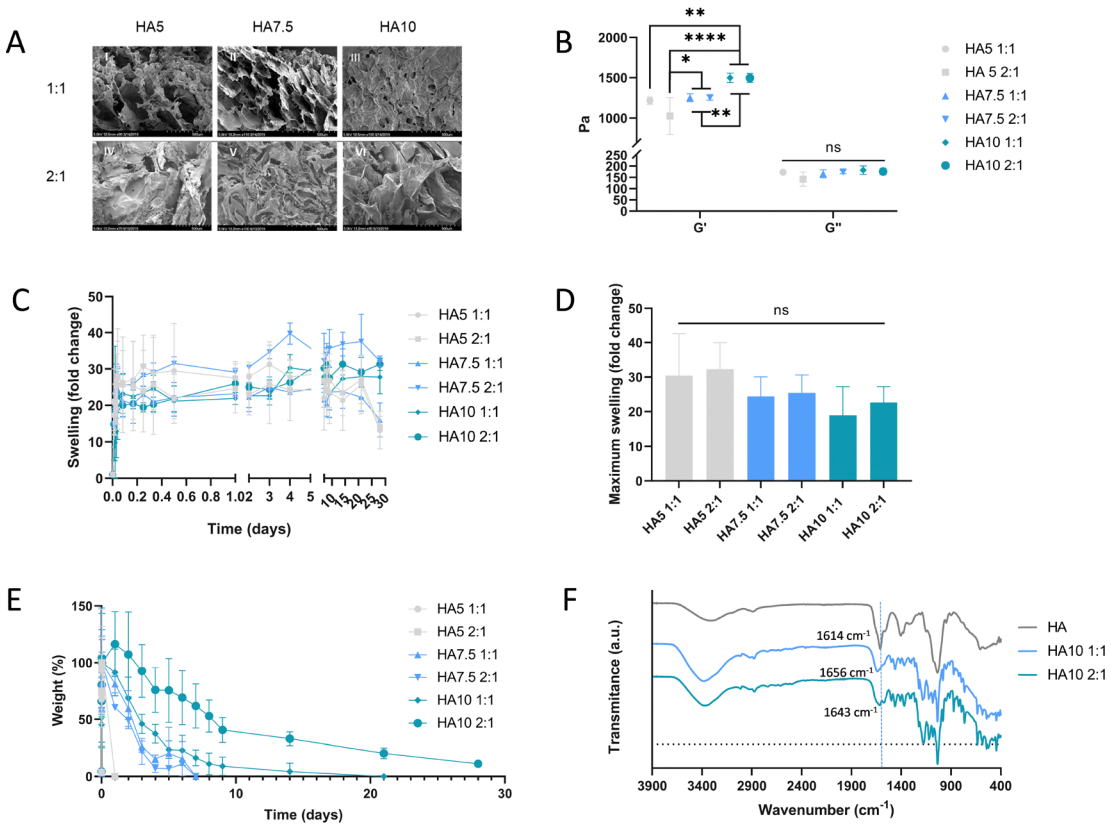

Fig. 1 HA-Based hydrogels presented constant swelling and stability over a month in ACSF: (A) SEM micrographs of hydrogel cross-section (scale bar = 500 μm); (B) storage (G′) and Loss (G″) modulus at 37 °C and 1 Hz. n = 6; data are presented as mean ± standard deviation. ANOVA, followed by Tukey's multiple comparison test * <0.05, ** <0.01, *** <0.005, and *** <0.001; ns means not significant (C) swelling in ACSF over time; (D) maximum swelling of the hydrogels in ACSF; data represented as mean ± standard deviation. ANOVA, followed by Tukey's multiple comparison test * <0.05, ** <0.01, *** <0.005, and *** <0.001; ns, not significant; (E) degradation in ACSF with 100 U mL^{-1} hyaluronidase. n = 6; data are presented as mean ± standard deviation. (F) FTIR spectra of naïve HA and the two more concentrated HA hydrogels. The highlighted band corresponds to the C═O stretching of the carboxylic group, with a clear shift to larger wavelengths after crosslinking with 4-arm-PEG-NH_2.

Thus, HMW HA was successfully cross-linked *via* a 4-arm PEG-NH_2 linker using DMTMM chemistry. A screening varying HA and 4-arm PEG-NH_2 concentrations and the ratio (w/w) among them on the final mixture was assessed in order to find the best properties for implantation of either intra-parenchymal or in the subarachnoid space. The microstructure of the engineered HA constructs, analyzed by SEM (Fig. 1A), demonstrated an apparent decrease in pore size with increasing concentrations of HA and PEG. This increased interconnectivity is related to efficient crosslinking, which leads to a more compact microstructure owing to the higher polymer concentration. The expected compact gel-like network was confirmed by rheological measurements, which determined the storage (G') and loss (G'') moduli (Fig. 1B). Having a larger storage modulus than the loss modulus indicates that elastic behavior governs the properties of the material.[11,16] All the formulations were analyzed at an oscillation frequency of 1 Hz, which is close to the human heart rate (~1.25 Hz), and at 37 °C. Brain storage modulus at 1 Hz ranges from 1–3 kPa.[17] Interestingly, the assessed HA constructs exhibited statistically significant G' values ranging from 0.7 to 1.5 kPa (Fig. 1B), from HA5 to HA10 formulations respectively. These values indicate the potential suitability of HA constructs to be safely implanted in the brain parenchyma or subarachnoid space without disturbing the host tissue integrity. However, the final effect of these mechanical properties on the healthy and pathological tissue would need to be elucidated in an *in vivo* scenario.

Furthermore, the swelling capacity of a hydrogel is a key property to consider when planning its implantation in the CNS. Swelling capacity, or the ability to absorb and reserve water, is the most distinctive property of hydrogels.[16] Thus, the polymeric network absorbs large quantities of liquid that is restricted by the presence of crosslinkers due to the retroactive forces of elasticity. Hence, varying the degree of HA-hydrogel crosslinking directly affected the swelling volume (Fig. 1C and D). The ability to absorb and retain ACSF was assessed over 28 days (Fig. 1C), and no significant differences were observed among the formulations tested. However, a trend was observed when analyzing the maximum swelling capacity at 24 h (Fig. 1D), which decreased when the polymer concentration increased. It should be noted that the formulations with 5 mg mL^{-1} HA concentration were capable of absorbing a larger volume in the first hours of incubation than those with higher HA concentrations, but were less efficient in retaining ACSF. This can be

explained by the fact that HA5 formulations have less or weak crosslinking, which results in expansion to a larger volume, while not retaining it. The ability to maintain a constant degree of swelling over a long period is crucial because it reflects the stability of the tested HA constructs. Hence, the tested formulations exhibited constant swelling behavior, which is potentially ideal for successful implantation without generating changes in tissue pressure over time. Moreover, HA10 formulations did not show any brittle behavior, which is generally associated to an undesirably high crosslinking degree.[18]

Polymer matrix biodegradation is one of the key mechanisms for successful application in the physiological milieu. Thus, degradation of the HA constructs was assessed over time at 37 °C in ACSF in the presence of a high concentration of hyaluronidase (Fig. 1E). As expected, the formulations containing a higher concentration of HA were more stable over time, with HA10 2 : 1 exhibiting a slower degradation profile. The formulations with 5 mg mL^{-1} HA concentration were completely degraded during the first day of incubation, while the 7.5 mg mL^{-1} had some remaining weight for one week. The two formulations with 10 mg mL^{-1} HA presented considerable remaining weight for at least 21 days, exhibiting the most promising degradation profile to be implemented in the biological milieu. Thus, these two formulations were chosen for biological assessment. Moreover, to confirm successful crosslinking, the hydrogels were analyzed by FTIR (Fig. 1F and Fig. S1, ESI†). As can be seen in the FTIR spectra of HA10 formulations, the –C═O stretching at 1614 cm^{-1} corresponds to the carboxyl groups of HA. After the chemical reaction with 4-arm-PEG-NH_2, the –C═O stretching peak shifted to larger wavenumbers (1656 cm^{-1} for HA10 1 : 1 and 1643 cm^{-1} for HA10 2 : 1), showing the characteristics of the carbon–oxygen vibration in the amide bonds. A similar shift was observed for the HA5 and HA7.5 formulations (Fig. S1, ESI†). This confirms the successful occurrence of chemical crosslinking.

3.2. HA10 cross-linked hydrogels performance on a relevant PCC *in vitro* model of neuroinflammation

The CNS is highly complex and involves microglia, astrocytes, oligodendrocytes, endothelial cells, and pericytes to maintain its homeostasis.[19] Neuroinflammation is mediated by reactive microglia and astrocytes. The interplay between them and neurons critically influences the responses to inflammatory insults. Despite the power of astrocyte and microglia monocultures to study specific molecular pathways involved in neuroinflammation, there is a lack of information related to crosstalk among cells.

Multicellular culture models have emerged as better models to overcome some of the drawbacks of single-cell culture in the context of CNS disorders, such as PD, spinal cord injury, or Stroke.[20–23] Therefore, we used PCC, a mixed population of cells found in the cortex, including microglia, astrocytes, neurons, and oligodendrocytes, to test the effect of HA formulations upon an inflammatory insult triggered by LPS. LPS induces a robust inflammatory response through Toll-Like Receptor 4 (TLR4). TLRs are widely expressed in CNS cells, and are upregulated in the pathological context of neurodegenerative diseases.[19]

After 7D in culture, PCC were exposed to LPS or complete DMEM, and after 24 h HA constructs were added to the culture (Fig. 2A). The effect of HA10 hydrogels on PCC was assessed 1, 3 and 7D after treatment, and their viability was assessed (Fig. 2 and Fig. S2, ESI†). As previously discussed, the HA5 and HA7.5 formulations were considerably degraded over time and exhibited poor mechanical properties, making them unsuitable for *in vitro* testing (Fig. S2, ESI†). Hence, the HA10 formulations were chosen for further studies. Hydrogels (100 mg) were added to the PCC, and metabolic activity (Fig. 2B), dsDNA content (Fig. 2C), and changes in the mixed population by ICC (Fig. 2D) were assessed over time. Interestingly, both HA10 formulations did not significantly affect metabolic activity or dsDNA content compared to the healthy control cells. However, LPS-triggered inflammation induced a statistically significant increase in metabolic activity and decreased dsDNA content. When treated with HA10 after LPS insult, these effects remained constant at 7D after the treatment and were slightly ameliorated by the HA10 2 : 1 formulation (Fig. 2C). Notably, these decreases in dsDNA content were negligible, and the differences were difficult to appreciate when analyzing the samples by ICC (Fig. 2D). The mixed population in the PCC remained constant throughout the study, with astrocytes (GFAP+ cells; Fig. 2E), microglia (Iba-1+ cells; Fig. 2F), neurons (β-tubulin III+ cells; Fig. 2G), and oligodendrocytes (Olig-2+ cells; Fig. 2H) present. It could be appreciated in the shape of the PCC, how the cells settle over the days in culture, reaching their suitable shape at 7D in culture, when they received the treatment.

3.3. HA10 formulations ameliorated LPS-induced inflammatory response on PCC

Microglia and astrocytes are key players in maintaining CNS homeostasis and resolving inflammatory processes, playing a pivotal role in regulating the immune response to pathological processes.[23] To study the effect of the two HA10 formulations in restoring the inflammatory state of the PCC in the acute phase after the LPS insult, cytokine release was assessed at 1D after the treatment (Fig. 3A–G). Hence, the release of pro-inflammatory cytokines (TNF-α, IL-1β, IL-6), anti-inflammatory cytokines (IL-4, IL-10, IL-13), and KC/GRO cytokines was analyzed after 24 h of treatment with HA10 formulations alone or pretreated with LPS. As expected, LPS-treated cells exhibited a higher release of pro-inflammatory cytokines such as TNF-α (Fig. 3A), IL-1β (Fig. 3B), and IL-6 (Fig. 3C). Interestingly, the release of TNF-α and IL-6 was significantly increased by the HA constructs after 24 h of treatment, suggesting a potential anti-inflammatory effect. In contrast, IL-4 release was significantly upregulated in PCC treated with HA10 constructs after the LPS inflammatory insult, indicating an anti-inflammatory effect mediated by HA (Fig. 3D). No differences were observed in the levels of the other cytokines assessed. Furthermore, nitrite concentration in the supernatant was analyzed as another indication of the inflammatory state of the culture (Fig. 3H). As expected, LPS triggered nitrite accumulation in the supernatant because of the inflammatory response. The concentrations were lower in all groups treated with HA10 formulations, either with or without LPS pretreatment, but without reaching significance.

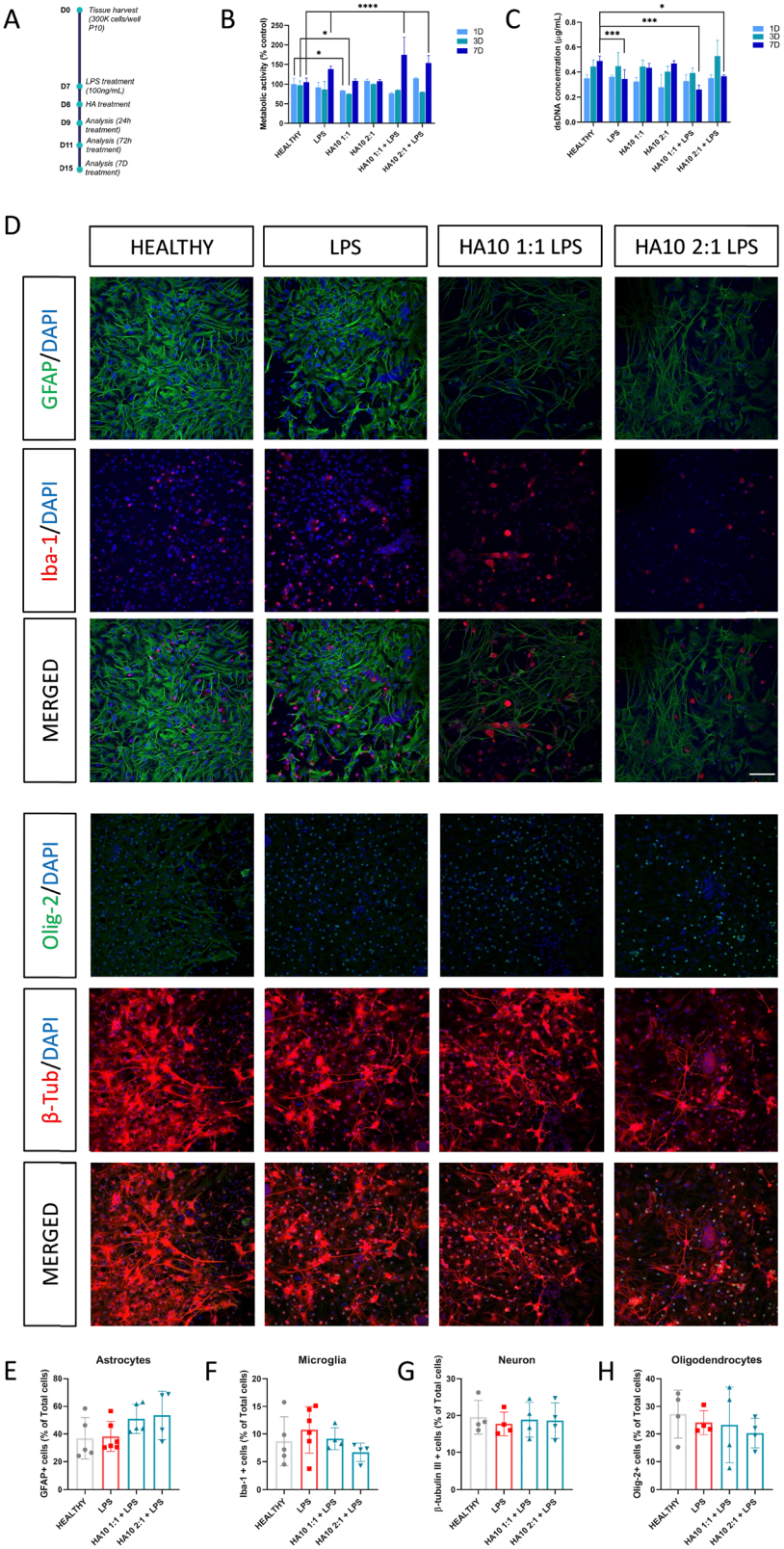

Fig. 2 Cross-linked HA10 is safe for PCC and does not alter the mixed population up to 7D after treatment: (A) flow chart of the *in vitro* model; (B) effect of HA10 on PCC (3×10^5 cells per well) metabolic activity determined by alamarBlue™ after 1, 3, and 7 days of exposure to the hydrogels. (C) dsDNA content after 1, 3, and 7 d of exposure to the hydrogels, as determined by Picogreen™. (D) Immunocytochemistry after seven days of treatment: glial fibrillary acidic protein (GFAP; astrocytes), ionized calcium-binding adapter molecule 1 (Iba-1; microglia), β-III-tubulin (β-Tub III; neurons), and Olig-2 (oligodendrocytes); data are representative of three independent experiments. Quantification of the percentages of (E) GFAP+, (F) Iba-1+, (G) β-III-tubulin+, and (H) olig-2+ cells with respect to the total number of cells. Data are presented as the mean ± standard deviation, $N > 4$; ANOVA, followed by Dunnett's multiple comparison test; * <0.05, ** <0.01, *** <0.005, and *** <0.001.

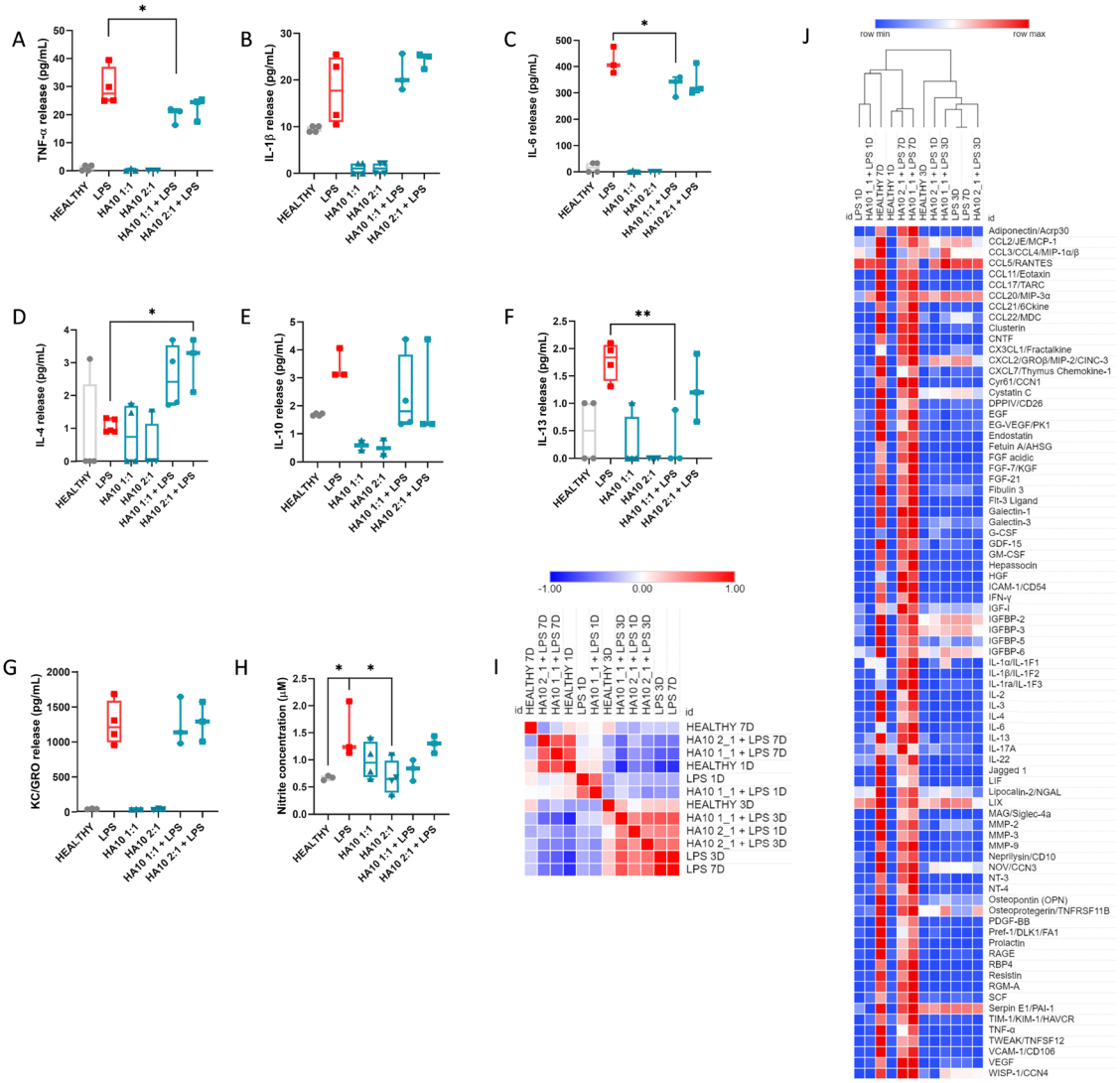

Fig. 3 Cross-linked HA reduces cytokine release in an LPS-induced inflammatory model of PCC: effect of HA10 on an LPS-induced inflammatory model in postnatal cortical cells. (A)–(G) Cytokine release and (H) nitrite concentration in the PCC supernatant after 24 h of treatment. The concentration of cytokines released into the supernatant was analyzed using multiplex ELISA. Data are represented as the mean ± standard deviation, $N = 4$. ANOVA followed by Dunnett's multiple comparison test; * <0.05; ** <0.01. (I) Similarity matrix extracted from (J) hierarchical clustering analysis of the 79 analytes. The mean pixel density was analyzed using a proteome profile array of proteins secreted by the PCC in the supernatant. Colors define activation as over-expressed (red) and under-expressed (blue). The supernatant was analyzed at three time points, day one, three and seven after treatment. The experiment was carried out in three biological replicates, and the supernatants were pooled to perform the proteome profiler array. Each analyte in the array was printed in duplicates. The values shown at each time point are the averages of both values.

To further understand HA10 effect on the inflammatory state of PCC, the culture supernatants were analyzed using a proteome profiler after 1D, 3D, and 7D treatments (Fig. 3I and J). The secretion of 79 crucial markers of neuroinflammation was analyzed over time. A hierarchical cluster analysis through Pearson's correlation was performed on the results obtained, showing different clusters of similarity. It can be seen in the similarity matrix (Fig. 3I) and in the clustered heatmap (Fig. 3H) that the PCC treated with HA10 formulations after LPS treatment, exhibited after 7D a similar inflammatory profile to that of Healthy PCC, which demonstrates the potential ability of the constructs to resolve inflammation during the chronic phase of culture. These differences were not detected in the early stages of treatment, when the HA10 formulations were not yet capable of restoring homeostasis. Some essential markers of neuroinflammation were significantly elevated during the acute phase (1D and 3D after treatment) after LPS treatment, when analyzing the semi-quantitative values of cytokine release (Fig. S3, ESI†). Chemokine (C–C motif) ligand 2 (CCL2) is expressed in astrocytes, endothelial cells, microglia, and neurons. Moreover, it is considered a key factor in the development of MS, with elevated serum levels found in MS patients.[24] After LPS treatment, CCL2 levels were clearly upregulated in PCC at 1D and 3D after treatment compared with the Healthy cells. These levels were downregulated in PCC treated with HA10. Other cytokines of the CCL family, such as CCL3 and CCL5, were also upregulated in

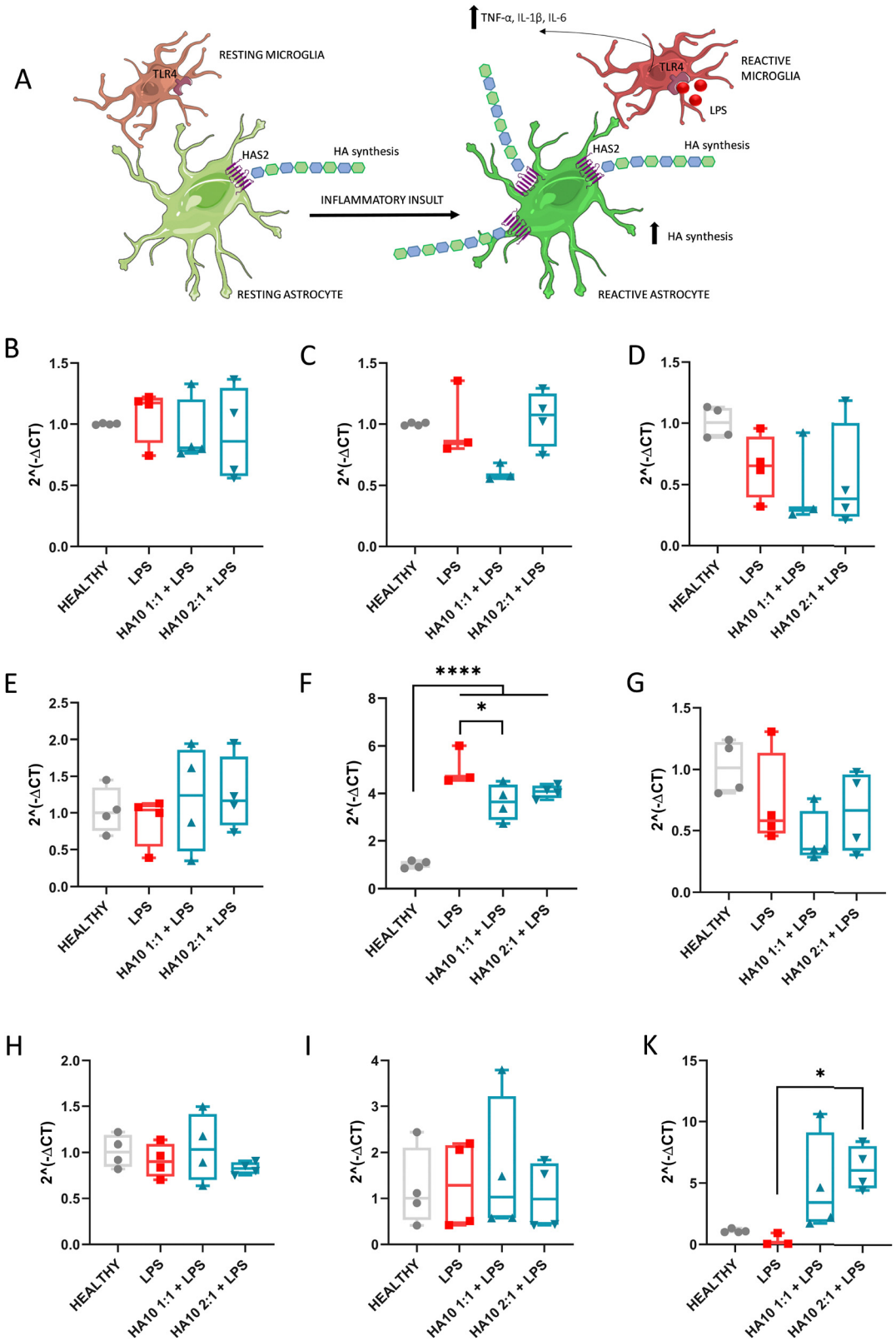

Fig. 4 Source of externally cross-linked HA has a direct effect on key players in HA metabolism 7 days after treatment. (A) Schematic representation of the HAS2 mediated synthesis of HA enhanced after inflammation in the cortex. Neuroinflammation related to hyaluronan metabolism – gene expression fold change (B)–(D) HYAL 1, 2 and 3 respectively; (E)–(G) HAS1, HAS2 and HAS3 respectively; (H) CD44, (I) RHAMM and (K) TSG6. Data are represented as mean ± standard deviation, $N = 4$. ANOVA followed by Dunnet multiple comparisons test * <0.05; ** <0.01; *** <0.005; *** <0.001.

LPS-treated PCC, proving the successful induction of a consistent inflammatory response similar to that observed in preclinical and clinical models of neuroinflammation associated with MS.[25,26] These β-chemokines are widely expressed by reactive microglia and astrocytes, whereas CCL5 is mainly expressed by endothelial cells and reactive astrocytes in response to inflammation. CCL chemokine release was considerably reduced in the acute phase of HA10 treatment, again demonstrating the potential of the hydrogels to efficiently ameliorate inflammation. Some key inflammatory players, such as IL-6 or IGFBP cytokines, were also downregulated by HA10 treatment after the inflammatory insult, further proving the anti-inflammatory activity of the constructs. In contrast, IL-1 family members, such as IL-1α and IL-1β, were upregulated by the LPS insult, further proving the robustness of the inflammatory induction; however, HA10 constructs did not reduce their release.

3.4. HA10 decreases inflammation-triggered HAS2 overexpression on PCC

Several questions regarding the role of HA in CNS development remain unanswered. However, HA has been shown to be critical not only during CNS development but also for its normal function. However, its role in neurodegeneration remains unclear. HA metabolism under homeostasis is orchestrated by the balance between hyaluronan synthases (HAS) and hyaluronidases (HYAL).[13] However, HA metabolism is dysregulated under pathological conditions in the brain.[4,6] HA is produced by three different transmembrane HAS, being HAS2 in charge of modulating its synthesis in the cerebral cortex.[7] After an inflammatory insult, HA synthesis by reactive astrocytes becomes upregulated in order to ameliorate inflammation (Fig. 4A).

In this study, we aimed to assess the effect of HA10 on the key players in hyaluronan metabolism in the cortex after an inflammatory insult. Thus, we analyzed the mRNA expression of HYAL 1, 2, and 3; HAS1, HAS2, and HAS3; and the HA receptors CD44, RHAMM, and TSG6 after 7 days of HA10 treatment (Fig. 4).

HA degradation is a highly complex process that can be driven enzymatically or by free radical reaction.[27] Enzymatic degradation is driven by endoglycosidases and exoglycosidases; however, the class that contributes the most is still unclear. Among endoglycosidases, the role on HA catabolism has been widely investigated.[27,28] Six isoforms of HYAL are known, but there is a consensus about the main role of HYALs 1–3 in the context of brain pathology. In this study, we analyzed their gene expression in the PCC culture for 7 days *in vitro* after the treatments (Fig. 4B–D). Three HYALs were expressed, but no differences were observed among the groups.

HA synthesis increases substantially at sites of injury or infection, and HA levels are greatly elevated in inflamed tissues.[13] Hence, the accumulation of HA in the CNS occurs as a result of HASes, but primarily reflects the activity of HAS1 and HAS2, with the latter being more prevalent in the cortex. Despite their structural similarity, HAS1 and HAS3 synthesize HA polymers of relatively small Mw (2×10^5–2×10^6 Da), while HAS2 synthesizes HA with an average Mw greater than 2×10^6 Da.[29] There is a substantial body of research reporting HAS2 as the major HA-producing enzyme.[30,31] Our results are consistent with this, showing that HAS1 (Fig. 4E) and HAS3 (Fig. 4G) expression is uniform among the experimental groups. In contrast, there was a 5-fold increase in the levels of HAS2 transcripts (Fig. 4F) after inflammatory insult. Interestingly, this expression was significantly downregulated when HA10 was administered 4- and 3-fold with respect to the healthy control, proving the potential effect of an external source of cross-linked HA to downregulate its synthesis by reactive astrocytes. The physiological effect of this downregulation warrants further investigation. Moreover, we assess the protein expression of the HAS1 (Fig. S4, ESI†) and HAS2 (Fig. S5, ESI†) through ICC, but the binding of both antibodies was to poor, with no significant differences appreciated even among Healthy and LPS-treated cells. Thus, these results were not relevant for the discussion due to technical limitations of the assessment.

Several proteins serve as HA receptors to transduce HA signaling, including CD44, RHAMM, lymphatic vessel endothelial hyaluronan receptor 1 (LYVE1), hyaluronic acid receptor for endocytosis (HARE), and toll-like receptors 2 and 4 (TLR2 and 4).[32] There is a general consensus that LMW-HA activates pro-inflammatory and proliferative signaling *via* TLR2/4 and CD44, whereas HMW-HA exhibits anti-proliferative and anti-apoptotic activities, potentially through a different conformation of CD44. The total amount of HA results from the balance of both larger and smaller sizes, with the phenotypic outcome resulting from the effects on receptor level of the differentially sized HA. CD44 is a polymorphic type I transmembrane glycoprotein with high diversity due to the splicing of more than 10 variable exons and glycosylation, which is specific for each cell type. The expression of CD44 was unaffected by the inflammatory insult or post-treatment with HA10 (Fig. 4H). CD44 protein expression was assessed through ICC, with no relevant immunostaining appreciated in any of the controls (Fig. S6, ESI†). The interaction between HA and CD44 receptors plays an important role in myelination and oligodendrocyte maturation during homeostasis, astrogliosis, and demyelination under pathological conditions. LPS did not trigger significant demyelination in the PCC *in vitro* model (Fig. S7, ICC MBP and βtub III, ESI†), but astrogliosis was evident after the inflammatory insult. Hence, an increase in CD44 expression was expected due to the inflammatory process but was not observed. This observation might be attributed to the slight LPS damage to the myelin sheets and oligodendrocytes, since CD44 overexpression is mainly attributed to glial cells surrounding demyelinated tissues or ischemic events.[33,34]

RHAMM, also known as CD168, binds to biotinylated HA and is thought to be involved in tumor cell locomotion and tissue repair after injury. RHAMM overexpression is mostly associated with tumor progression.[35] HA catabolism, which generates smaller fragments of the polymer, triggers regenerative responses mainly mediated through HA-RHAMM interactions.[13,35] However, differences in gene expression were not observed among groups.

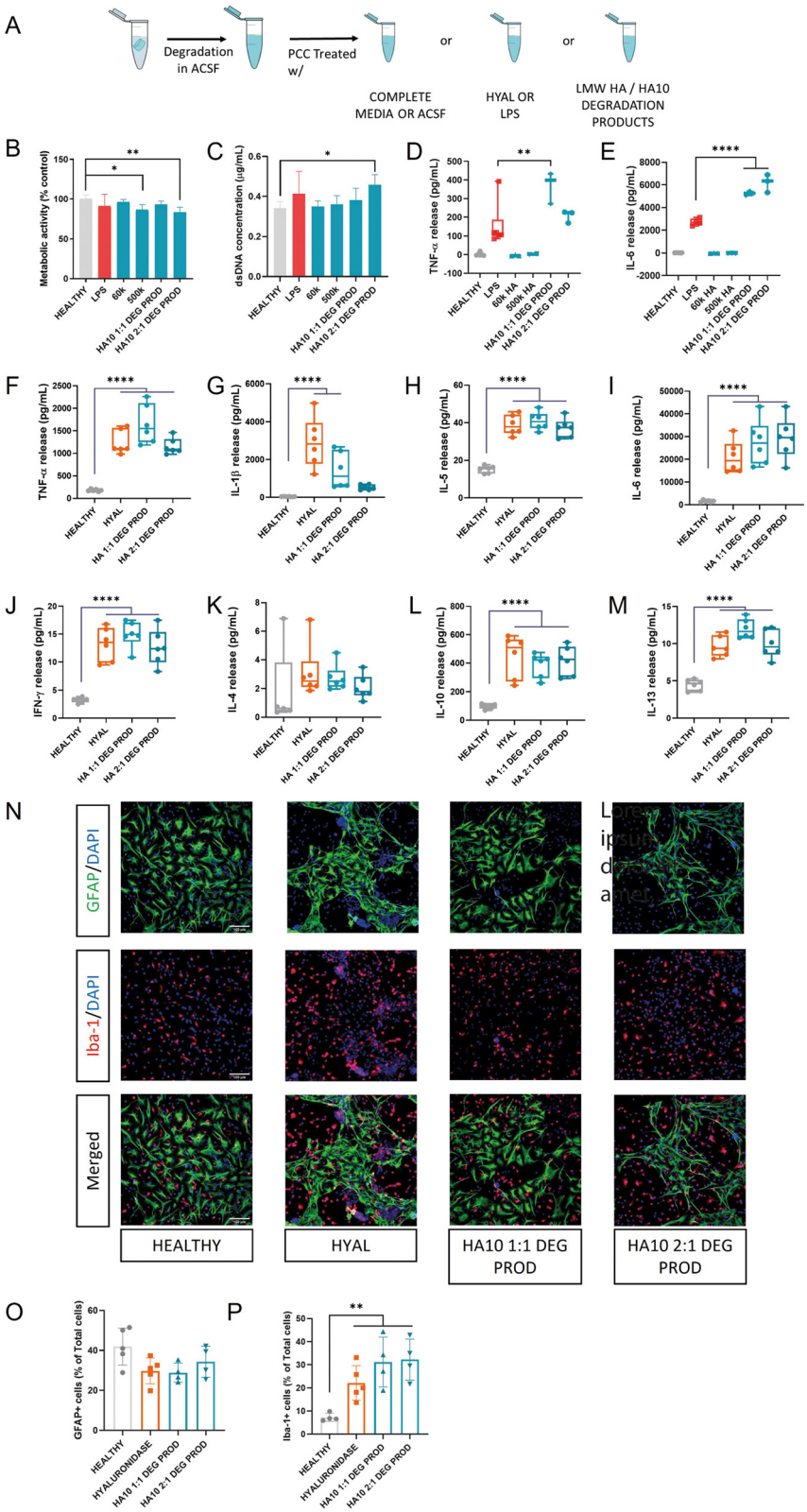

Fig. 5 Effect of HA hydrogel degradation products on the PCC mixed population. (A) Scheme of the workflow used to assess the effect of HA degradation products on the PCC after 24 h of exposure. (B) Effect of HA10 degradation products and LMW HA on PCC metabolic activity determined using alamarBlue™ after 1 d of exposure to HA10 degradation products or LMW HA. (C) dsDNA content determined by Picogreen™ after 1 d of exposure to HA10 degradation products; (D)–(M) cytokine release in PCC supernatant after 24 h treatment. Cytokine concentrations released into the supernatant were analyzed using ELISA (D)–(E) data presented as mean ± standard deviation, $N > 3$; and multiplex ELISA (F)–(M). Data are presented as the mean ± standard deviation, $N = 6$. ANOVA followed by Dunnett's multiple comparison test * <0.05, ** <0.01, *** <0.005, and *** <0.001. (N) Immunocytochemistry after one day of treatment; GFAP (astrocytes) and Iba-1 (microglia); data representative of three independent experiments. Quantification of the % of (O) GFAP+ and (P) Iba-1+ cells with respect to the total number of cells. Data are presented as the mean ± standard deviation, $N \geq 3$. ANOVA followed by Dunnet multiple comparisons test * <0.05; ** <0.01; *** <0.005; *** <0.001.

TSG-6 is an HA-binding protein of the group of hyaladherins constitutively expressed on the adult CNS, which catalyzes the covalent transfer of heavy chains (HCs) (also known as HA-associated protein SHAP) from inter-alpha-trypsin inhibitor (IαI) to HA under inflammation.[36] The resulting HC-HA complex induces a shift from pro-inflammatory to anti-inflammatory phenotype in macrophages, therefore playing a key role in the resolution of inflammation.[37] TSG-6 levels have been reported to be downregulated in autoimmune disorders with an inflammatory component, and our results are in consonance with the decrease in its expression after LPS treatment (Fig. 4K). Interestingly, TSG-6 mRNA was overexpressed after HA10 treatment, most probably due to the presence of high HA in the biological matrix, potentially coordinating and stabilizing the interaction with the HA-rich matrix. This effect is consistent with the downregulation of inflammatory markers after 7 days, most probably due to the shift of glial cells to an anti-inflammatory phenotype.

3.5. HYAL-cleaved HA10 degradation products but not LMW HA exert an inflammatory response on PCC

HMW HA is present in most tissues under homeostasis, and its steady-state turnover is thought to be mediated mostly by tissue macrophages.[38] However, LMW HA is present under pathological conditions, mainly inflammation. There is a living debate regarding the role of these HA fragments as a cause of the inflammatory response or a consequence of inflammation. The overall body of research has shown that the administration of HMW HA in a wide variety of inflammation-mediated diseases leads to an anti-inflammatory response. On the contrary, LMW HA (>500 kDa) have been reported of inducing pro-inflammatory responses through CD44 or TLR4, their combination or TLR2.[39]

Despite the general consensus regarding the role of size in the final biological effect, some concerns have been raised. Various recent studies have reported no effect of LMW HA or HA fragments on different models of inflammation *in vitro*[40] and *in vivo*.[38,41] Thus, we assessed the effect of the degradation products of HA10 on PCC, using 60 kDa and 500 kDa HA as controls (Fig. 5). HA10 cells were incubated with bovine HYAL (100 U mL^{-1}) until they were completely degraded. Then, the HA10 solution was used as a treatment and PCC was exposed to it for 24 h (Fig. 5A). Metabolic activity significantly decreased in cells exposed to 500 kDa HA and HA10 2 : 1 degradation products, but was always above 70% (Fig. 5B). Interestingly, no detrimental effect was observed in terms of dsDNA content for any of the treatments, further proving the safety of HA10 degradation products (Fig. 5C). However, when TNF-α (Fig. 5D) and IL-6 (Fig. 5E) release was assessed, cells treated with HA10 degradation product showed a significant increase when compared with the LPS-treated group, while the PCC treated with LMW HA showed no release. Hence, we decided to test the effect of HYAL in the supernatant of the HA10 degradation products to evaluate the role of the enzyme on the pro-inflammatory response (Fig. 5F–N). For this reason, we assessed the proinflammatory profile of PCC treated with HA10 degradation products using HYAL-treated cells as a control. Interestingly, a similar pro-inflammatory profile in terms of the cytokines released and their concentration in the supernatant was observed for the HYAL-treated group and HA10 degradation products, as determined by multiplex ELISA (Fig. 5F–N). Moreover, we assessed the changes in the glial cell population using ICC (Fig. 5N). No significant difference was observed in the number of astrocytes (Fig. 5O). However, the percentage of microglial cells increased significantly after exposure to hyaluronidase or HA10 degradation products (Fig. 5P), which was in line with the increased cytokine release. This effect is probably related to the pro-inflammatory effect induced by HYAL at high doses which directly affects the overall PCC population. Altogether, our results are in agreement with those recent reports claiming the lack of pro-inflammatory effects of LMW HA, suggesting that the presence of endotoxins, hyaluronidase, or other substances in the HAs tested might play a key role in the previously reported inflammation-triggered response. However, a more in-depth analysis using HA of different molecular weights, and from different sources, as well as a screening of HYAL concentrations, must be conducted to understand the mechanisms behind these effects in a robust manner.

4. Conclusions

We have proved that cross-linked HA-based hydrogels have a key effect on inflammatory onset in an *in vitro* model of cortical neuroinflammation using PCC. Moreover, HA10 efficiently downregulated gliosis, reducing the severity of the inflammatory response after seven days of treatment, exhibiting an inflammatory phenotype similar to that of healthy cells. Furthermore, the downregulation of intrinsic HA synthesis through HAS2 could potentially have an effect on neuroinflammatory onset, preventing its deposition and scar generation in demyelinated axons. However, our model presents limitations in this sense, since LPS-triggered inflammation does not affect myelin sheets as other chemicals such as lysolecithin do, and the culture itself does not present mature myelinated axons. Further experiments, particularly in *in vivo* models of inflammation and demyelination, are necessary to validate the impact of HA10 constructs in resolving inflammation by modulating hyaluronan metabolism in preclinical settings. Moreover, *in vivo* studies would shed light on the spatio-temporal changes of HA synthases in the onset of neuroinflammation, which is another limitation of the current study. In addition, physicochemical parameters such as viscosity or injectability of HA10 or other HA-based constructs should be taken into consideration in the preclinical stage. Herein, HA10 was used to maximize the HA concentration and its effect *in vitro*, making it possible to analyze its effect on inflammation resolution and HA metabolism in depth. Thus, we set a promising baseline for the use of HA-based hydrogels to treat neuroinflammatory processes through the modulation of the brain ECM. If our findings are proven in preclinical models of neuroinflammation, new approaches targeting ECM remodelling through HA-metabolism managing could exhibit big clinical potential to tackle neuroinflammatory-driven diseases.

In conclusion, we shed some light on the living debate about the potential dual effect of HA-based materials on the CNS depending on its molecular weight, showing that LMW HA had no detrimental or pro-inflammatory effect on the PCC. Our results showed that the pro-inflammatory effect may be due to the presence of hyaluronidase, endotoxins, or other substances. Altogether, our results contribute to the baseline knowledge regarding the use of HA-based materials in the context of the CNS in cortical inflammatory disorders.

Author contributions

S. M.-S. and A. P. conceptualized and designed the study. S. M.-S. performed the experiments, wrote and revised the article. M. A.-W. and M. T. C. performed the experiments and worked on the edited version of the article. E. B. and C. L. performed the RT-PCR experiments and analysis, and contributed to the revised version of the manuscript. Y. B. helped on the experimental design and characterization of the materials, and contributed to the revised version of the manuscript. U. F. helped in the conceptualization and contributed to the revised version of the manuscript. A. P. supervised and directed the project. All authors critically reviewed and approved the final manuscript.

Data availability

All data associated with this study are present in the paper or the ESI.† The raw data that support the findings of this study is available from the corresponding authors upon reasonable request.

Conflicts of interest

Authors declare no conflict of interest.

Acknowledgements

This publication has emanated from research supported partly by a grant from the Research Ireland and is co-funded under the European Regional Development Fund under Grant number 13/RC/2073_P2. This work was funded by the European Union Horizon 2020 Programme (H2020-MSCA-IF-2017) under the Marie Skłodowska-Curie Individual Fellowship Grant Agreement No. 797716. This project has received funding from the European Union's Horizon 2020 Research and Innovation Programme under the Marie Skłodowska-Curie grant agreement no. 713690. This project has received funding from the European Union's Horizon 2020 research and innovation programme under the Marie Skłodowska-Curie Grant agreement no. 813263. The authors acknowledge the facilities and scientific and technical assistance of the Centre for Microscopy & Imaging at the University of Galway (**https://imaging.universityofgalway.ie/imaging/**).

References

1 C. K. Glass, K. Saijo, B. Winner, M. C. Marchetto and F. H. Gage, Mechanisms underlying inflammation in neurodegeneration, *Cell*, 2010, **140**(6), 918–934.
2 P. M. Matthews, Chronic inflammation in multiple sclerosis—Seeing what was always there, *Nat. Rev. Neurol.*, 2019, **15**(10), 582–593.
3 J. L. Milstein, C. R. Barbour, K. Jackson, P. Kosa and B. Bielekova, Intrathecal, not systemic inflammation is correlated with Multiple Sclerosis severity, especially in Progressive Multiple Sclerosis, *Front. Neurol.*, 2019, **10**, 1232.
4 S. A. Back, T. M. Tuohy, H. Chen, N. Wallingford, A. Craig, J. Struve, N. L. Luo, F. Banine, Y. Liu and A. Chang, Hyaluronan accumulates in demyelinated lesions and inhibits oligodendrocyte progenitor maturation, *Nat. Med.*, 2005, **11**(9), 966–972.
5 J. D. Crapser, J. Ochaba, N. Soni, J. C. Reidling, L. M. Thompson and K. N. Green, Microglial depletion prevents extracellular matrix changes and striatal volume reduction in a model of Huntington's disease, *Brain*, 2020, **143**(1), 266–288.
6 T. Srivastava, L. S. Sherman and S. A. Back, Dysregulation of Hyaluronan Homeostasis During White Matter Injury, *Neurochem. Res.*, 2020, **45**(3), 672–683.
7 H. F. Kuipers, M. Rieck, I. Gurevich, N. Nagy, M. J. Butte, R. S. Negrin, T. N. Wight, L. Steinman and P. L. Bollyky, Hyaluronan synthesis is necessary for autoreactive T-cell trafficking, activation, and Th1 polarization, *Proc. Natl. Acad. Sci. U. S. A.*, 2016, **113**(5), 1339–1344.
8 G. Safarians, A. Sohrabi, I. Solomon, W. Xiao, S. Bastola, B. W. Rajput, M. Epperson, I. Rosenzweig, K. Tamura and B. Singer, Glioblastoma Spheroid Invasion through Soft, Brain-Like Matrices Depends on Hyaluronic Acid–CD44 Interactions, *Adv. Healthcare Mater.*, 2023, **12**(14), 2203143.
9 W. Su, S. Matsumoto, B. Sorg and L. S. Sherman, Distinct roles for hyaluronan in neural stem cell niches and perineuronal nets, *Matrix Biol.*, 2019, **78**, 272–283.
10 N. G. Kotla, S. R. Bonam, S. Rasala, J. Wankar, R. A. Bohara, J. Bayry, Y. Rochev and A. Pandit, Recent advances and prospects of hyaluronan as a multifunctional therapeutic system, *J. Controlled Release*, 2021, **336**, 598–620.
11 I. Perez-Estenaga, M. T. Chevalier, E. Peña, G. Abizanda, A. M. Alsharabasy, E. Larequi, M. Cilla, M. M. Perez, J. Gurtubay, M. Garcia-Yebenes Castro and A. Multimodal, Scaffold for SDF1 Delivery Improves Cardiac Function in a Rat Subacute Myocardial Infarct Model, *ACS Appl. Mater. Interfaces*, 2023, **15**(44), 50638–50651.
12 A. Mathew, J. M. Pakan, E. C. Collin, W. Wang, K. W. McDermott, U. Fitzgerald, R. Reynolds and A. S. Pandit, An ex-vivo multiple sclerosis model of inflammatory demyelination using hyperbranched polymer, *Biomaterials*, 2013, **34**(23), 5872–5882.
13 N. Nagy, H. F. Kuipers, P. L. Marshall, E. Wang, G. Kaber and P. L. Bollyky, Hyaluronan in immune dysregulation and autoimmune diseases, *Matrix Biol.*, 2019, **78**, 292–313.
14 N. Schizas, R. Rojas, S. Kootala, B. Andersson, J. Pettersson, J. Hilborn and N. P. Hailer, Hyaluronic acid-based hydrogel

enhances neuronal survival in spinal cord slice cultures from postnatal mice, *J. Biomater. Appl.*, 2014, **28**(6), 825–836.
15 I. L. M. Isa, S. A. Abbah, M. Kilcoyne, D. Sakai, P. Dockery, D. P. Finn and A. Pandit, Implantation of hyaluronic acid hydrogel prevents the pain phenotype in a rat model of intervertebral disc injury, *Sci. Adv.*, 2018, **4**(4), eaaq0597.
16 S. Martin-Saldana, M. Al Waeel, A. M. Alsharabasy, A. Daly and A. Pandit, An interdisciplinary framework for the characterization of extracellular matrix-hydrogels for biomedical applications, *Matter*, 2022, **5**(11), 3659–3705.
17 C. F. Guimarães, L. Gasperini, A. P. Marques and R. L. Reis, The stiffness of living tissues and its implications for tissue engineering, *Nat. Rev. Mater.*, 2020, **5**(5), 351–370.
18 P. Kesharwani, A. Bisht, A. Alexander, V. Dave and S. Sharma, Biomedical applications of hydrogels in drug delivery system: an update, *J. Drug Delivery Sci. Technol.*, 2021, **66**, 102914.
19 W. Zhang, D. Xiao, Q. Mao and H. Xia, Role of neuroinflammation in neurodegeneration development, *Signal Transduction Targeted Ther.*, 2023, **8**(1), 267.
20 N. Goshi, R. K. Morgan, P. J. Lein and E. Seker, A primary neural cell culture model to study neuron, astrocyte, and microglia interactions in neuroinflammation, *J. Neuroinflammation*, 2020, **17**, 1–16.
21 V. Patil, E. O'Connell, L. R. Quinlan, H. Fearnhead, S. McMahon and A. Pandit, A robust platform for high-throughput screening of therapeutic strategies for acute and chronic spinal cord injury, *iScience*, 2021, **24**(3), 102182.
22 E. Bagnoli, A. Trotier, J. McMahon, L. R. Quinlan, M. Biggs, A. Pandit and U. FitzGerald, Prodromal Parkinson's disease and the catecholaldehyde hypothesis: insight from olfactory bulb organotypic cultures, *FASEB J.*, 2023, **37**(12), e23272.
23 M. T. Chevalier, M. Al-Waeel, A. M. Alsharabasy, A. L. Rebelo, S. Martin-Saldaña and A. Pandit, Therapeutic Polymer-Based Cannabidiol Formulation: Tackling Neuroinflammation Associated with Ischemic Events in the Brain, *Mol. Pharm.*, 2024, **21**(4), 1609–1624.
24 J. L. Madrigal and J. R. Caso, The chemokine (CC motif) ligand 2 in neuroinflammation and neurodegeneration, *Oxidative Stress and Inflammation in Non-communicable Diseases-Molecular Mechanisms and Perspectives in Therapeutics*, 2014, pp. 209–219.
25 R. Chui and K. Dorovini-Zis, Regulation of CCL2 and CCL3 expression in human brain endothelial cells by cytokines and lipopolysaccharide, *J. Neuroinflammation*, 2010, **7**, 1–12.
26 G. M. Arisi, M. L. Foresti, K. Katki and L. A. Shapiro, Increased CCL2, CCL3, CCL5, and IL-1β cytokine concentration in piriform cortex, hippocampus, and neocortex after pilocarpine-induced seizures, *J. Neuroinflammation*, 2015, **12**, 1–7.
27 M. M. Kasper, B. Ellenbogen, Y. Li and C. E. Schmidt, Temporal characterization of hyaluronidases after peripheral nerve injury, *PLoS One*, 2023, **18**(8), e0289956.
28 A. Katarzyna Greda and D. Nowicka, Hyaluronidase inhibition accelerates functional recovery from stroke in the mouse brain, *J. Neurochem.*, 2021, **157**(3), 781–801.
29 N. Itano, T. Sawai, M. Yoshida, P. Lenas, Y. Yamada, M. Imagawa, T. Shinomura, M. Hamaguchi, Y. Yoshida and Y. Ohnuki, Three isoforms of mammalian hyaluronan synthases have distinct enzymatic properties, *J. Biol. Chem.*, 1999, **274**(35), 25085–25092.
30 M. Valkonen, H. Haapasalo, K. Rilla, K. Tyynelä-Korhonen, Y. Soini and S. Pasonen-Seppänen, Elevated expression of hyaluronan synthase 2 associates with decreased survival in diffusely infiltrating astrocytomas, *BMC Cancer*, 2018, **18**, 1–11.
31 D. R. Michael, A. O. Phillips, A. Krupa, J. Martin, J. E. Redman, A. Altaher, R. D. Neville, J. Webber, M.-Y. Kim and T. Bowen, The Human Hyaluronan Synthase 2 (HAS2) Gene and Its Natural Antisense RNA Exhibit Coordinated Expression in the Renal Proximal Tubular Epithelial Cell, *J. Biol. Chem.*, 2011, **286**(22), 19523–19532.
32 D. Vigetti, E. Karousou, M. Viola, S. Deleonibus, G. De Luca and A. Passi, Hyaluronan: biosynthesis and signaling, *Biochim. Biophys. Acta, Gen. Subj.*, 2014, **1840**(8), 2452–2459.
33 C. Reinbach, M.-S. Stadler, N. Pröbstl, U. Chrzanowski, C. Schmitz, M. Kipp and T. Hochstrasser, CD44 expression in the cuprizone model, *Brain Res.*, 2020, **1745**, 146950.
34 R. Sawada, A. Nakano-Doi, T. Matsuyama, N. Nakagomi and T. Nakagomi, CD44 expression in stem cells and niche microglia/macrophages following ischemic stroke, *Stem Cell Invest.*, 2020, **7**, 4.
35 M. A. Pibuel, D. Poodts, Y. Molinari, M. Díaz, S. Amoia, A. Byrne, S. Hajos, S. Lompardía and P. Franco, The importance of RHAMM in the normal brain and gliomas: physiological and pathological roles, *Br. J. Cancer*, 2023, **128**(1), 12–20.
36 V. J. Coulson-Thomas, M. E. Lauer, S. Soleman, C. Zhao, V. C. Hascall, A. J. Day and J. W. Fawcett, Tumor necrosis factor-stimulated gene-6 (TSG-6) is constitutively expressed in adult central nervous system (CNS) and associated with astrocyte-mediated glial scar formation following spinal cord injury, *J. Biol. Chem.*, 2016, **291**(38), 19939–19952.
37 A. J. Day and C. M. Milner, TSG-6: a multifunctional protein with anti-inflammatory and tissue-protective properties, *Matrix Biol.*, 2019, **78**, 60–83.
38 Y. Dong, A. Arif, M. Olsson, V. Cali, B. Hardman, M. Dosanjh, M. Lauer, R. J. Midura, V. C. Hascall and K. L. Brown, Endotoxin free hyaluronan and hyaluronan fragments do not stimulate TNF-α, interleukin-12 or upregulate co-stimulatory molecules in dendritic cells or macrophages, *Sci. Rep.*, 2016, **6**(1), 36928.
39 F. T. Zakusilo, M. K. O'Banion, H. A. Gelbard, A. Seluanov and V. Gorbunova, Matters of size: roles of hyaluronan in CNS aging and disease, *Ageing Res. Rev.*, 2021, **72**, 101485.
40 D. Krejcova, M. Pekarova, B. Safrankova and L. Kubala, The effect of different molecular weight hyaluronan on macrophage physiology, *Neuroendocrinol. Lett.*, 2009, **30**(1), 106.
41 Z. Huang, C. Zhao, Y. Chen, J. A. Cowell, G. Wei, A. Kultti, L. Huang, C. B. Thompson, S. Rosengren and G. I. Frost, Recombinant human hyaluronidase PH20 does not stimulate an acute inflammatory response and inhibits lipopolysaccharide-induced neutrophil recruitment in the air pouch model of inflammation, *J. Immunol.*, 2014, **192**(11), 5285–5295.

